Sensitivity of the Tropospheric Circulation to Changes in the Strength of the Stratospheric Polar Vortex

THOMAS JUNG

ECMWF, Reading, United Kingdom

JAN BARKMEIJER

KNMI, De Bilt, Netherlands

ABSTRACT

The sensitivity of the wintertime tropospheric circulation to changes in the strength of the Northern Hemisphere stratospheric polar vortex is studied using one of the latest versions of the ECMWF model. Three sets of experiments were carried out: one control integration and two integrations in which the strength of the stratospheric polar vortex has been gradually reduced and increased, respectively, during the course of the integration. The strength of the polar vortex is changed by applying a forcing to the model tendencies in the stratosphere only. The forcing has been obtained using the adjoint technique. It is shown that, in the ECMWF model, changes in the strength of the polar vortex in the middle and lower stratosphere have a significant and slightly delayed (on the order of days) impact on the tropospheric circulation. The tropospheric response shows some resemblance to the North Atlantic Oscillation (NAO), though the centers of action are slightly shifted toward the east compared to those of the NAO. Furthermore, a separate comparison of the response to a weak and strong vortex forcing suggests that to first order the tropospheric response is linear within a range of realistic stratospheric perturbations. From the results presented, it is argued that extended-range forecasts in the European area particularly benefit from the stratosphere–troposphere link.

1. Introduction

The possibility of an influence of the wintertime stratospheric polar vortex on the tropospheric circulation has been a topic of increasing interest in recent years. This is because such a link, if existent, implies some predictability of the atmospheric circulation well into the extended range (from about 10 days to one season). The reasoning is based on the observation that the stratospheric polar vortex varies relatively slowly compared to the tropospheric circulation (Baldwin et al. 2003). As a consequence, if the stratospheric polar vortex is, for example, anomalously strong, then its temporal persistence suggests that it is likely to remain strong for some time into the near future. Therefore, if the polar vortex would have a significant impact on the tropospheric circulation, then this would increase the

memory of the troposphere leaving it potentially more predictable.

The possibility of an influence of the stratospheric polar vortex on the tropospheric circulation during wintertime is of considerable interest to operational forecasting centers. This is particularly true for the European Centre for Medium-Range Weather Forecasts (ECMWF), where monthly ensemble forecasts with a coupled atmosphere–ocean model are routinely being carried out once a week since autumn 2004 (Vitart 2004), and it is monthly forecasting that is likely to benefit the most from a possible stratosphere–troposphere coupling.

The recent increase of interest in stratosphere–troposphere coupling has largely been fueled by two observational studies (Baldwin and Dunkerton 1999, 2001). Baldwin and Dunkerton showed that stratospheric anomalies of the Arctic Oscillation (AO: Thompson and Wallace 1998), which reflect changes in the stratospheric polar vortex, appear to "propagate" downward into the troposphere, thereby changing the

Corresponding author address: Dr. Thomas Jung, ECMWF, Shinfield Park, Reading RG2 9AX, United Kingdom.
E-mail: thomas.jung@ecmwf.int

strength of the midlatitude westerly winds as well as the strength and location of the storm tracks.

The predictive skill associated with the downward "propagation" has been estimated by Charlton et al. (2003) and Baldwin et al. (2003) using statistical models. Both studies conclude that the stratosphere–troposphere link provides some extra skill in statistically forecasting Northern Hemisphere weather.

The stratosphere–troposphere link has also been investigated using numerical models of the atmosphere. The first such study was carried out by Boville (1984) in an attempt to quantify the impact that inaccuracies in simulations of the stratosphere have on the tropospheric model climate. The "inaccuracy" in the stratosphere was generated by changing the stratospheric diffusion. Boville found significant tropospheric changes compared with a control integration, the response of which closely resembles the spatial structure of the North Atlantic Oscillation (NAO). Similar studies have been carried out more recently (Polvani and Kushner 2002; Norton 2003; Taguchi 2003), basically confirming the original results by Boville.

In each of the modeling studies described above the stratospheric circulation has been altered by changing the model formulation. Charlton et al. (2004) have pointed out a potential shortcoming of this approach, namely, that changes in model formulation may lead to an unrealistic stratospheric climate compared to that of the control integration. Moreover, Charlton et al. highlighted that only the time-mean response has been studied although it is the transient response that is more closely related to the forecasting problem. To circumvent the aforementioned problems, Charlton et al. (2004) decided to study the influence of changes of the initial conditions (see also Kodera et al. 1991) in the stratosphere in the ECMWF model leaving the model formulation unchanged. As in the other modeling studies described above, Charlton et al. (2004) found a significant tropospheric response resembling the NAO. To achieve this response, however, they had to introduce substantial changes to the initial conditions. Moreover, even the relatively large number of integrations considered—ensemble integrations encompassing 50 members were used—does not mitigate the fact that only three cases were considered.

In this study we revisit the stratosphere–troposphere link by means of numerical experimentation using one of the most sophisticated atmospheric circulation models, the ECMWF model, which is operationally being used to carry out medium-range and extended-range forecasts. As in Charlton et al. (2004), we focus on the transient response of the troposphere to perturbations of the stratospheric polar vortex in order to address the predictability problem. However, instead of introducing a rather drastic change to the initial conditions, we efficiently perturb the model equations in the stratosphere only leaving the initial conditions and model dynamics unchanged. The forcing applied is based on the adjoint technique. Moreover, the relatively large sample size—sixty 40-day integrations were carried out—ensures that reliable conclusions can be drawn. Finally, a novelty of the present study is that strong and weak polar vortex cases are considered separately in order to test the linearity of the tropospheric response for a range of realistic stratospheric perturbations.

The paper is organized as follows. In the following section the ECMWF model used in this study is briefly described. Moreover, the method used to construct the forcing, which is used to change the stratospheric polar vortex, is outlined. (Details are given in the appendix.) The results are presented in section 3, which includes diagnosis of the zonally averaged zonal-mean wind response as well as changes of the horizontal circulation at three pressure levels (50, 500, and 1000 hPa). Moreover, the response of the tropospheric transient eddies is studied. This is followed by an investigation on how the tropospheric response depends on the actual flow. Finally, the main findings of this study will be summarized and discussed.

2. Methods

a. Experimental design

To study the sensitivity of the tropospheric circulation to changes in the strength of the stratospheric polar vortex three sets of numerical experiments were carried out:

$$d\mathbf{x}^i/dt = G(\mathbf{x}^i), \tag{1}$$

$$d\mathbf{x}^i/dt = G(\mathbf{x}^i) + \mathbf{F}, \tag{2}$$

$$d\mathbf{x}^i/dt = G(\mathbf{x}^i) - \mathbf{F}, \tag{3}$$

where $\mathbf{x}^i$ describes the time-dependent atmospheric state vector; superscript $i = 1, \ldots, K$ denotes the ith forecast experiment ($K = 60$ cases in this study); G symbolizes the dynamical and physical part of the ECMWF model (see next subsection for details); and $\mathbf{F}$ is a *small* and *constant* forcing that is constructed to change the strength of the stratospheric polar vortex in the Northern Hemisphere (see appendix for details). The forcing is zero throughout the troposphere. The first set of experiments form the unperturbed control integration (CNTL hereafter); the second and third sets
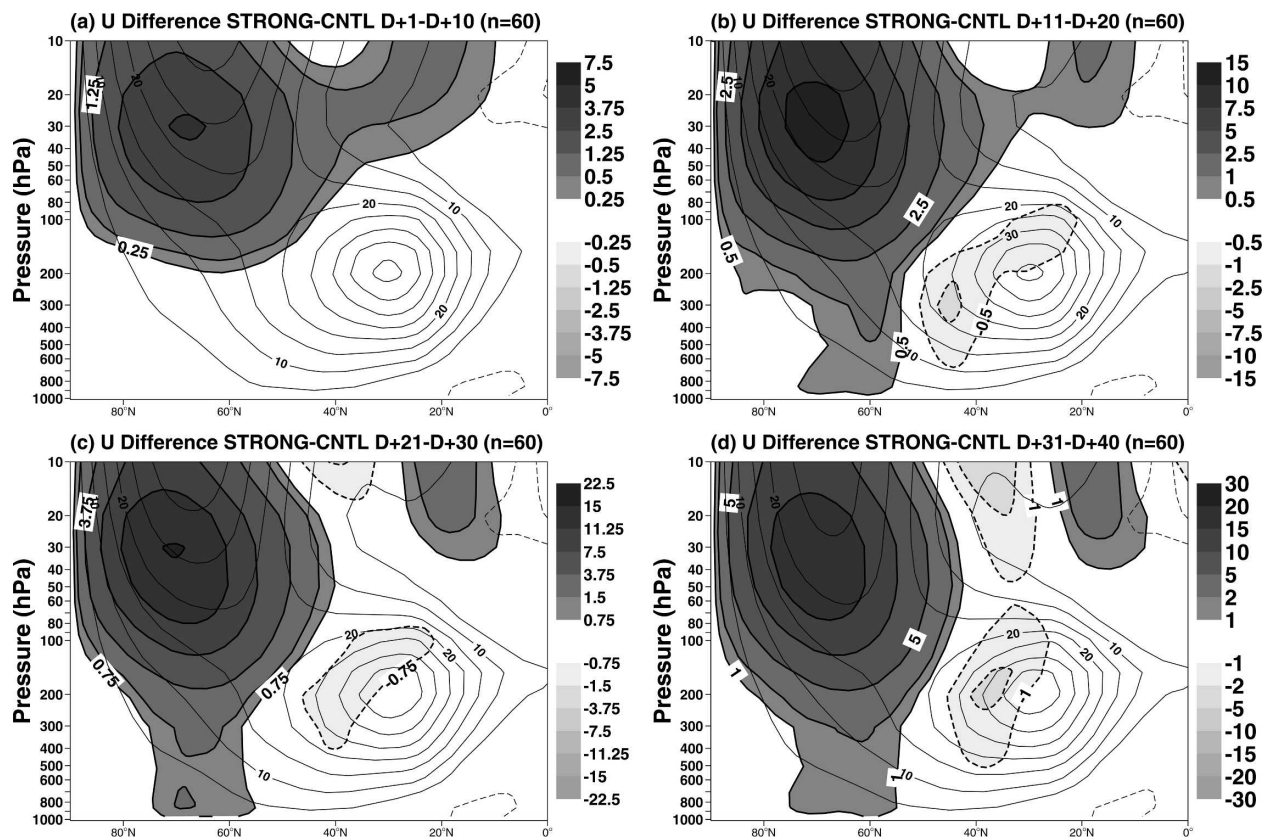
FIG. 1. Difference of average zonal-mean zonal winds (shading in m s^{-1}) between the strong polar vortex (STRONG) and the control experiment (CNTL) for 10-day averages: (a) $D + 1$ to $D + 10$, (b) $D + 11$ to $D + 20$, (c) $D + 21$ to $D + 30$, and (d) $D + 31$ to $D + 40$. Shown is the average over 60 different cases (40-day integrations). Notice that the contour interval for the differences changes linearly with the forecast range. Also shown are zonal-mean zonal winds from the control integration (contour interval is 5 m s^{-1}).

form experiments in which the strength of the polar vortex has been increased (STRONG hereafter) and reduced (WEAK hereafter), respectively, by applying the forcing **F** during the course of the integration.

For each of the three experiment types (CNTL, STRONG, and WEAK) a total of sixty D + 40 forecasts[1] were carried out; the forecasts were started on 1 December, 1 January, and 1 February of each of the winters from 1981/82 to 2000/01. The fact that the initial dates are at least one month apart takes into account the rather persistent character of stratospheric anomalies (Baldwin et al. 2003) and ensures that each of the sixty 40-day forecasts represents an independent realization, thus increasing the robustness of the results.

Throughout the remainder of this section the ECMWF model is described in brevity. Details on how

the optimal forcing **F** has been computed are given in the appendix.

b. Model

The model, G, used to carry out the nonlinear integrations is one of the latest versions of the ECMWF model (cycle 28r1) that has been used operationally from 9 March to 27 September 2004. In this study a horizontal resolution of T_L95 (linear Gaussian grid, $\approx 1.875°$) is used and 60 levels in the vertical are employed. About half of the levels are located above the tropopause; that is, the vertical resolution of the stratosphere is relatively high (e.g., Untch and Simmons 1999). The highest model level is located at about 0.1 hPa. Some aspects of the model performance at this resolution, including the stratosphere, are discussed elsewhere (Jung and Tompkins 2003; Jung 2005). In particular the study by Jung and Tompkins (2003) shows that the model climate in the lower and middle stratosphere agrees very well with estimates from the ECMWF 40-yr Re-Analysis (ERA-40).

---

[1] As is common practice in the numerical weather prediction community, we shall use the expression D + n forecast for an n-day forecast.
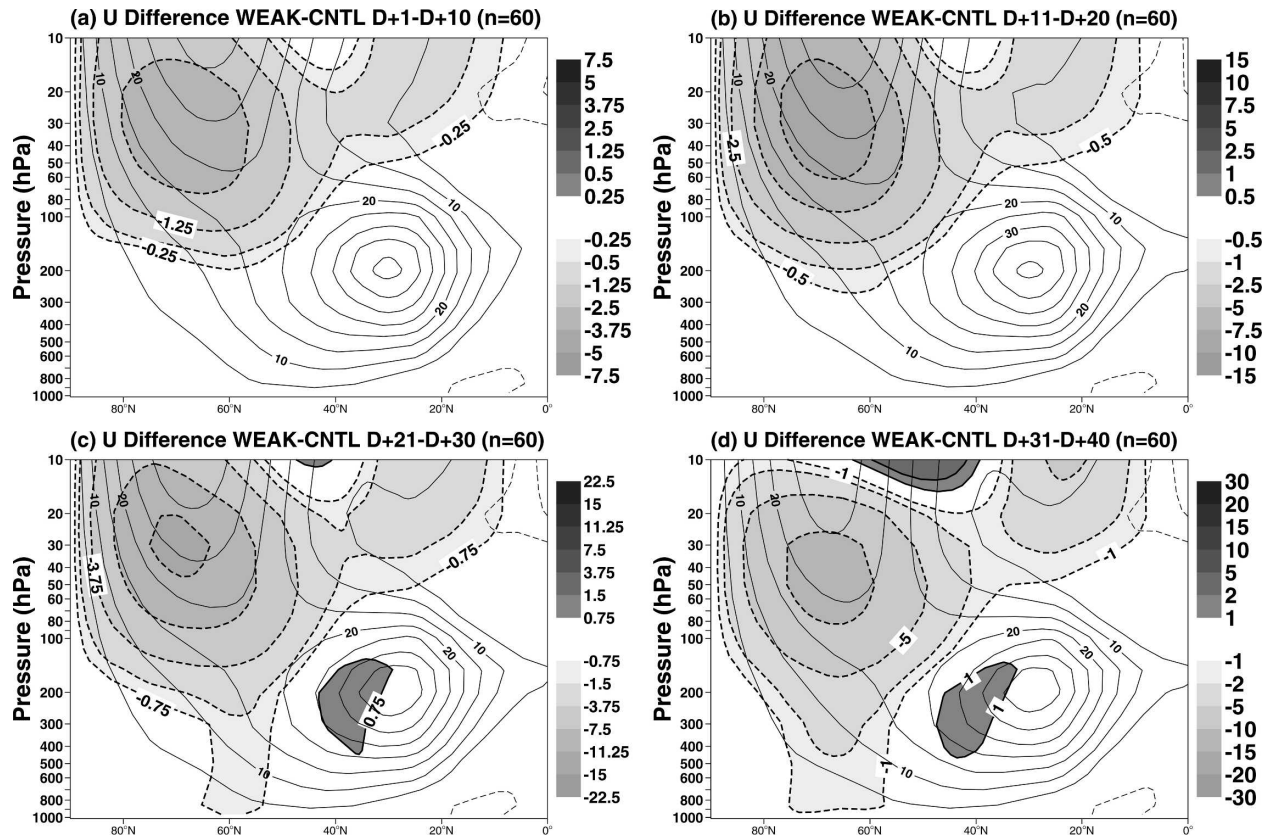
FIG. 2. As in Fig. 1 except for the difference between experiment WEAK (weak vortex) and CNTL (control).

3. Results

a. Zonal-mean zonal winds

Changes in the strength of the stratospheric polar vortex have a strong zonally symmetric component. Thus, an effective way to evaluate the experiments described in the previous section is to consider zonal-mean zonal winds. The differences of the averaged (over all 60 cases) zonal-mean zonal winds between STRONG and CNTL is shown in Fig. 1 for four different forecast ranges, that is, for averages from $D + 1$ to $D + 10$, $D + 11$ to $D + 20$, $D + 21$ to $D + 30$, and $D + 31$ to $D + 40$. Also shown are average zonal-mean zonal winds for the control integration CNTL. The first thing to notice is that the forcing $\mathbf{F}$, which is based on the adjoint technique, is very efficient in changing the strength of stratospheric polar vortex. The maximum change is found around 30 hPa. Moreover, the stratospheric perturbation growth (STRONG minus CNTL) is more or less linear in time. During the last 10 days of the integration ($D + 31$ to $D + 40$) the polar vortex in STRONG is almost twice as strong as that in CNTL.

Differences of the average zonal-mean zonal wind are also evident in the Northern Hemisphere tropo-

sphere, at least after 10 days or so into the integration. These changes encompass an increase of the zonal-mean westerly winds between 50° and 70°N (polar jet stream) and a decrease of the subtropical jet at its northern flank. In the Northern Hemisphere midlatitudes the increase of zonal-mean winds in STRONG amounts to about 10%–20% of the average zonal-mean winds in CNTL. From the above diagnostics it is evident that, by construction, $\mathbf{F}$ is very efficient in altering the circulation in the stratosphere. Furthermore, a relatively strong response is found in the Northern Hemisphere troposphere, where the forcing $\mathbf{F}$ is zero. This shows that the wintertime tropospheric circulation in the ECMWF model is, indeed, sensitive to changes in the strength of the stratospheric polar vortex.

The difference of the average zonal-mean zonal winds between WEAK and CNTL is shown in Fig. 2. The strength of polar vortex in the former experiment is clearly weakened compared to the control integration. During the last 10 days of the 40-day integrations the polar vortex has almost completely collapsed at around 50 hPa. Furthermore, it is evident that the difference between WEAK and CNTL is virtually the same as that for the difference between STRONG and

(a) Z50 Difference STRONG-CNTL D+1-D+10

(b) Z50 Difference STRONG-CNTL D+11-D+20

(c) Z50 Difference STRONG-CNTL D+21-D+30
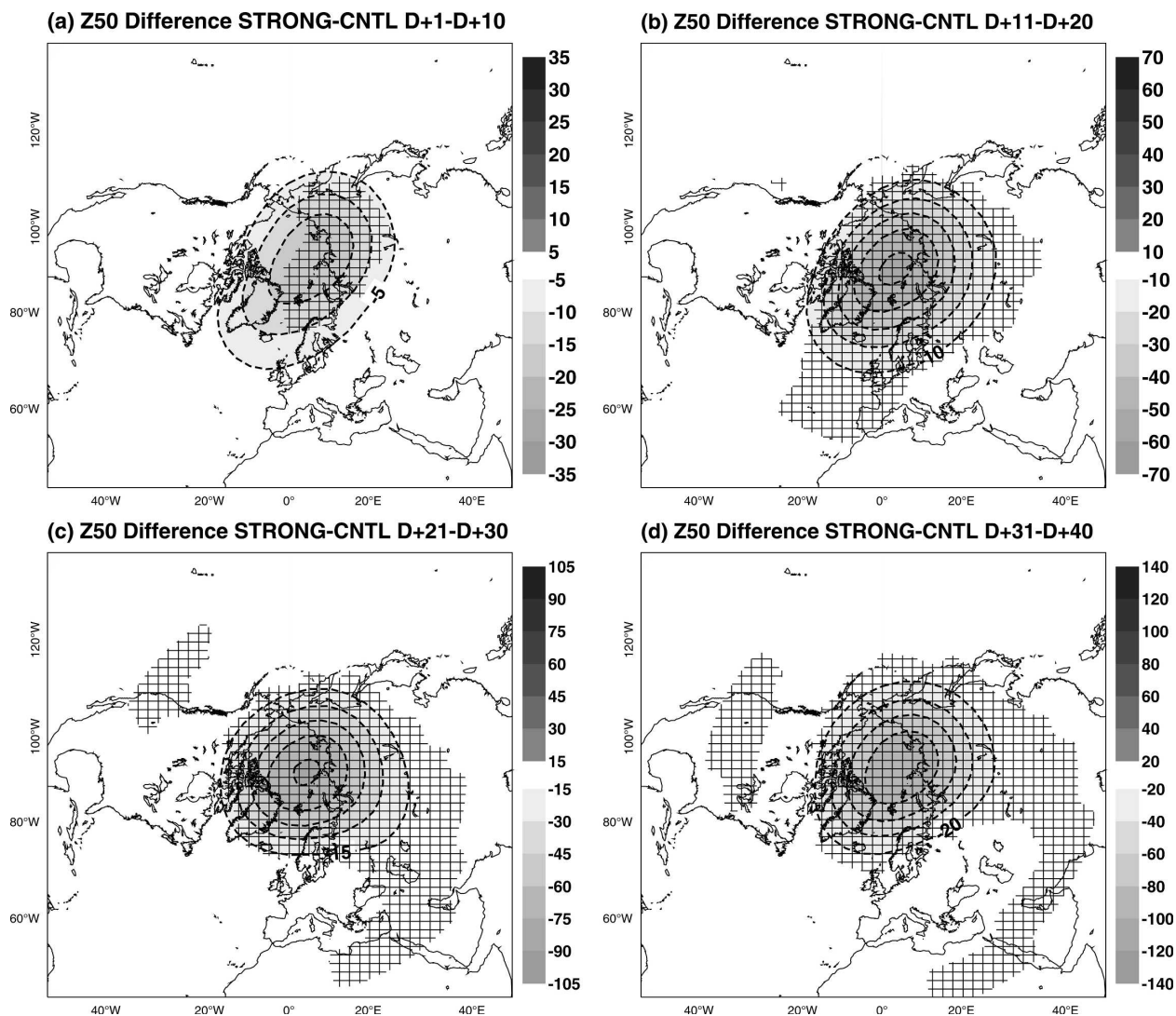
(d) Z50 Difference STRONG-CNTL D+31-D+40

FIG. 3. Difference of 50-hPa geopotential height (shading in dam) between the strong polar vortex (STRONG) and the control experiment (CNTL) for 10-day averages: (a) $D + 1$ to $D + 10$, (b) $D + 11$ to $D + 20$, (c) $D + 21$ to $D + 30$, and (d) $D + 31$ to $D + 40$. Shown is the mean over 60 different cases (40-day integrations). Notice that the contour interval for the differences changes linearly with the forecast range. Differences that are statistically significant at the 95% confidence level (two-sided Student's t test) are hatched.

CNTL, both in the stratosphere and the troposphere, except for the expected change in sign. This resemblance implies that the response to the forcing **F** is largely linear.

b. Mean geopotential height fields

After having described the vertical structure of the zonally symmetric response of the ECMWF model to changes in the strength of the polar vortex, in the following the response of the horizontal circulation will be discussed in more detail.

The difference of mean geopotential height fields at

50 hPa (Z_{50}, hereafter) between STRONG and CNTL is shown in Fig. 3. The forcing **F** leads to a pronounced and statistically significant strengthening of the polar vortex. The evolved perturbation grows at an approximately linear rate throughout the forecast, and during the last 10 days of the integration ($D + 31$ to $D + 40$) Z_{50} in STRONG is lower by about 800 m over the Arctic compared to CNTL.

The experiment WEAK, with $-$**F** applied during the integration, shows the same response in Z_{50}, except for opposite signs (Fig. 4). The character of the stratospheric response to the forcing **F**, therefore, is largely linear.

(a) Z50 Difference WEAK-CNTL D+1-D+10

(b) Z50 Difference WEAK-CNTL D+11-D+20

(c) Z50 Difference WEAK-CNTL D+21-D+30

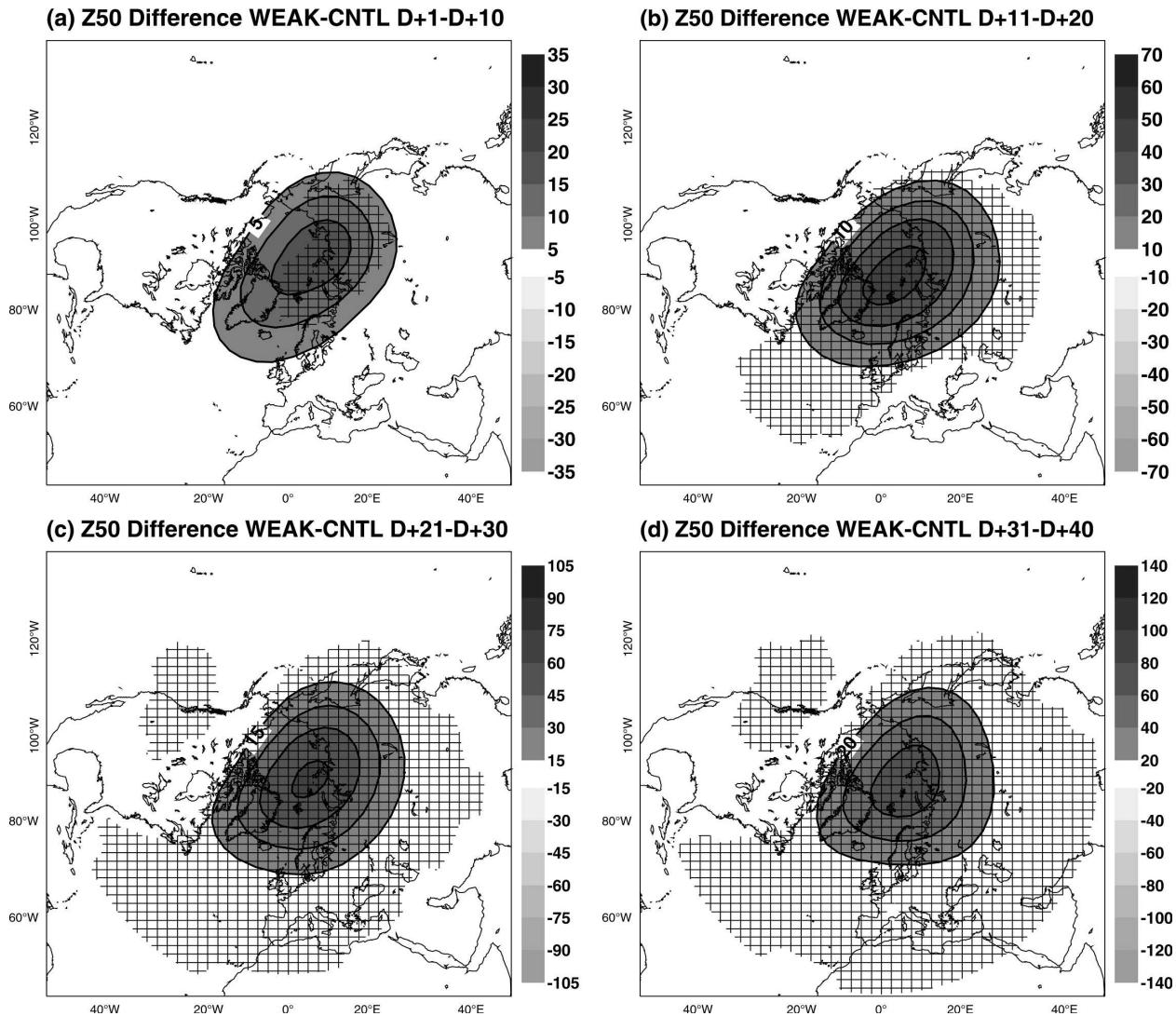**(d) Z50 Difference WEAK-CNTL D+31-D+40**

FIG. 4. As in Fig. 3 but for the difference between experiment WEAK (weak vortex) and CNTL (control).

Next, the response of geopotential height fields at 500 hPa (Z_{500}, hereafter) is investigated. The difference of average Z_{500} between STRONG and WEAK is shown in Fig. 5. Three main centers of action stand out. Anomalously low values of Z_{500} are found for STRONG in the Greenland/Iceland area, whereas positive Z_{500} differences are evident over Europe and East Asia. No significant response is found in the North Pacific region and over North America. This implies that the response of zonal-mean zonal winds in the midlatitude troposphere (see Fig. 1) is largely due to zonal wind changes in the North Atlantic region and large parts of Eurasia. The Z_{500} differences between STRONG and CNTL further show that the perturbation growth is relatively small during the first 10 days or so compared to later forecast ranges (see below). Fi-

nally, it is worth mentioning that the Z_{500} response to a stratospheric forcing shows some resemblance to the NAO, although the Z_{500} dipole is somewhat shifted to the east compared to the usual pattern of the NAO.

The Z_{500} difference between WEAK and CNTL (Fig. 6) resembles the response to a strong polar vortex except for a change in sign. This also suggests that the tropospheric response at 500 hPa to changes in the strength of the stratospheric polar vortex is basically linear. There are differences in the response between STRONG and WEAK, however, which may be due to sampling variability; the signal-to-noise ratio of the tropospheric response is lower than that in the stratosphere (not shown).

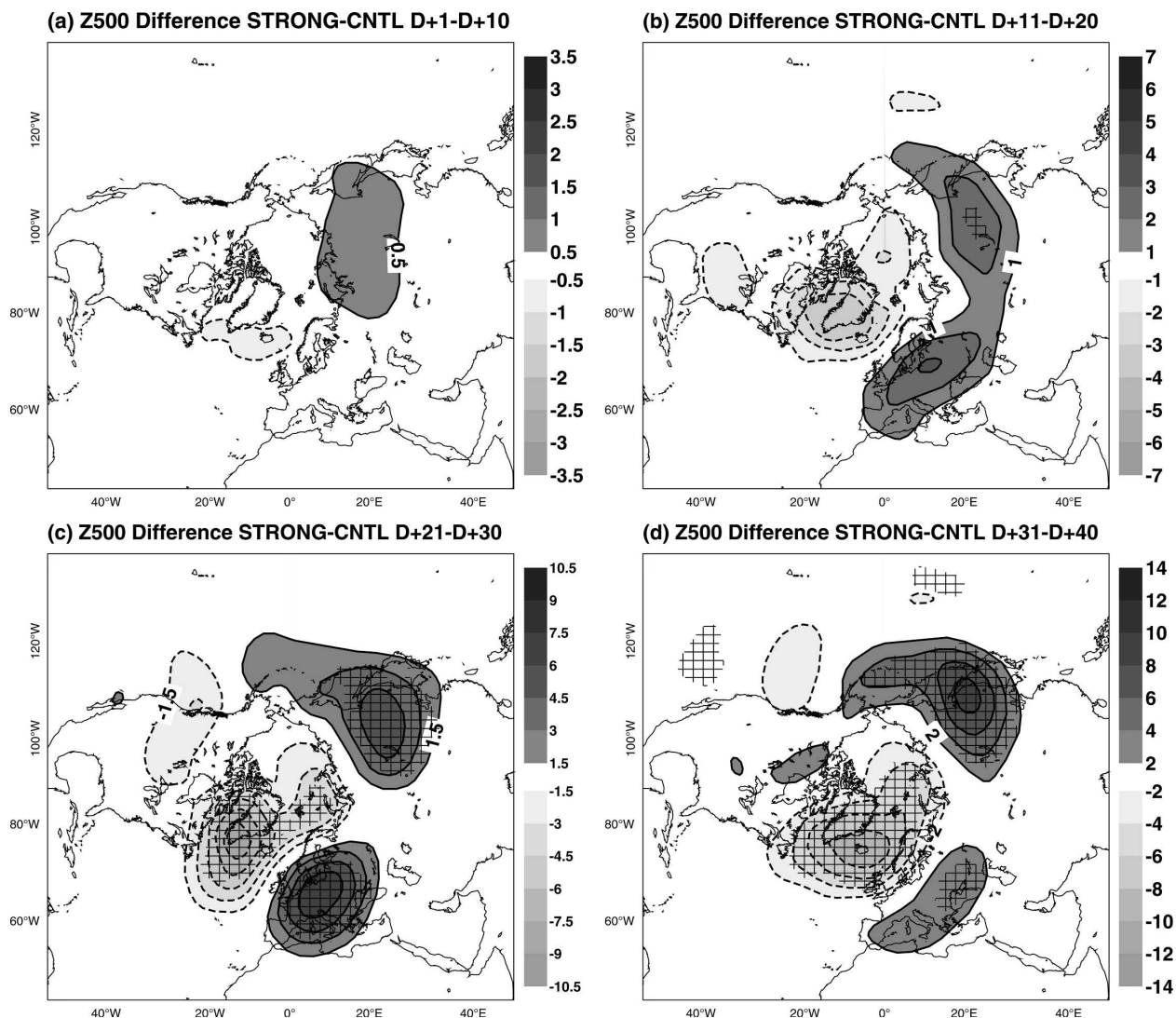The response of the horizontal circulation close to the surface can be inferred from Fig. 7, which shows the

(a) Z500 Difference STRONG-CNTL D+1-D+10

(b) Z500 Difference STRONG-CNTL D+11-D+20

(c) Z500 Difference STRONG-CNTL D+21-D+30

(d) Z500 Difference STRONG-CNTL D+31-D+40

FIG. 5. As in Fig. 3 but for the 500-hPa level.

difference of geopotential height fields at the 1000-hPa level (Z_{1000}, hereafter) between STRONG and CNTL. Close to the surface, the largest and statistically significant response is found in the northeastern North Atlantic and parts of the Arctic, at least after more than 20 days into the integration. Interestingly, the strongest initial response ($D + 1 - D + 10$) occurs in the Greenland/Icelandic area, that is, an area where the NAO has its northern center of action.

As for the 50- and 500-hPa level the experiment WEAK shows virtually the same response as STRONG, except for opposite signs (Fig. 8). This also suggests that the near-surface response to changes in the strength of the stratospheric polar vortex is basically linear with respect to the sign of the stratospheric forcing.

It has been briefly mentioned above that there are

differences in the rate at which the magnitude of tropospheric perturbations grow during the course of the integration. This result is further substantiated by Fig. 9, which shows the evolution of the magnitude of the Northern Hemispheric response, expressed in terms of the Euclidean norm, throughout the forecast at three different vertical levels (50, 500, and 1000 hPa). Note that results are based on the difference between STRONG and WEAK. Up to $D + 15$ or so, the tropospheric response grows at a lower rate than that in the stratosphere; thereafter the growth in the stratosphere and troposphere is comparable. The exact cause of the delayed tropospheric response is not known. One might speculate, however, that this delay is due to some downward propagation of the strongest perturbation from the middle to the lower stratosphere. Moreover, it

(a) Z500 Difference WEAK-CNTL D+1-D+10

(b) Z500 Difference WEAK-CNTL D+11-D+20

(c) Z500 Difference WEAK-CNTL D+21-D+30

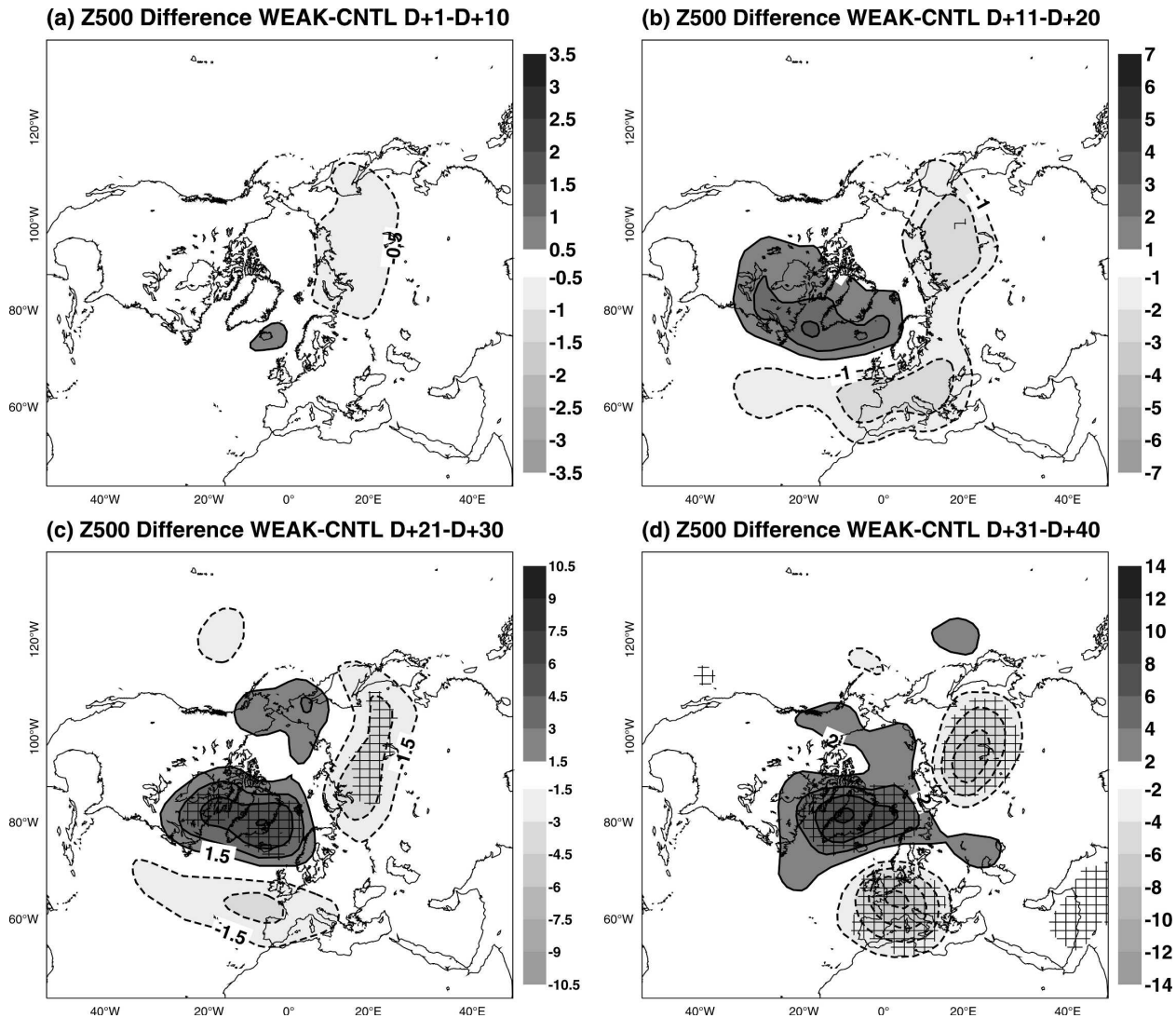**(d) Z500 Difference WEAK-CNTL D+31-D+40**

FIG. 6. As in Fig. 4 but for the 500-hPa level.

is conceivable that nonlinear eddy–mean flow interactions in the troposphere are responsible for the delayed accelerated response around $D + 15$ (see below).

c. Synoptic-scale transients

The difference of synoptic Z_{500} activity in the range from $D + 21$ to $D + 30$ between STRONG and WEAK is shown in Fig. 10. Here, synoptic activity is computed by taking the standard deviation of day-to-day Z_{500} changes. As pointed out by Jung (2005), this filter is particularly useful if high-pass filtering has to be carried out for short time series (10-day segments in this study). The largest and statistically significant impact of the stratospheric forcing is found over northern Europe and the northeastern North Atlantic, highlighting the fact that extended-range forecasts for the European re-

gion should benefit the most from the stratosphere–troposphere link. Moreover, as shown by Ting and Lau (1993) and Hurrell (1995b) the vorticity fluxes associated with an increased storm track are such to induce a horizontal cyclonic (anticyclonic) circulation to its north (south). In this way, the eddies could indeed positively feed back onto the mean large-scale tropospheric anomaly.

Recently, it has been suggested that the stratospheric influence on the troposphere is, in fact, mediated by the transient eddies (Charlton et al. 2004; Wittman et al. 2004). This is in contrast to earlier proposed mechanisms of the tropospheric response focusing on large-scale dynamics (e.g., Black 2002; Ambaum and Hoskins 2002). To help understand the tropospheric response in the experiments described in this study, average
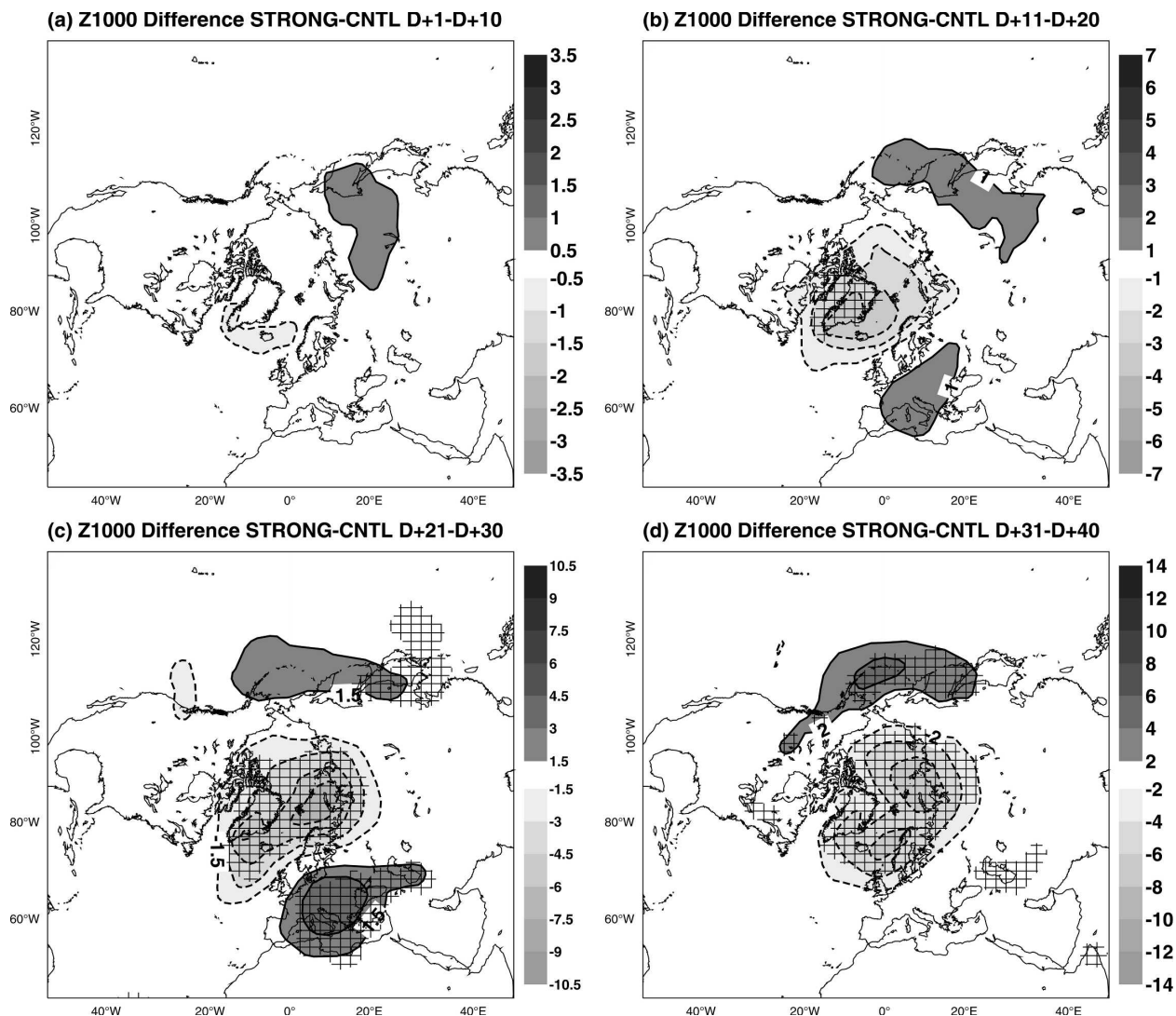
(a) Z1000 Difference STRONG-CNTL D+1-D+10

(b) Z1000 Difference STRONG-CNTL D+11-D+20

(c) Z1000 Difference STRONG-CNTL D+21-D+30

(d) Z1000 Difference STRONG-CNTL D+31-D+40

FIG. 7. As in Fig. 3 but for the 1000-hPa level.

spatial spectra have been computed at $D + 2$, $D + 4$, $D + 10$, and $D + 20$ from Z_{500} difference fields between STRONG and WEAK (Fig. 11, solid line). Also shown are 95% confidence intervals (using a χ^2 test, shading). Initially, that is, at $D + 2$ and $D + 4$, the strongest tropospheric response is found on relatively large spatial scales. This suggests that it is large-scale dynamics and not dynamics on synoptic scales (approximately wavenumber 7–15) that is crucial for initially mediating the link between the stratosphere and troposphere.

d. Climatology of stratospheric vortex variability

The experiment WEAK shows a strong weakening of the polar vortex as reflected by Z_{50} anomalies in excess

of 700 m beyond $D + 30$ (Figs. 4c,d). The corresponding near-surface response in terms of Z_{1000} amounts to about 60 m (Figs. 4c,d), which is equivalent to a mean sea level pressure anomaly of about 6 hPa. It is natural to ask how realistic such anomalies of the stratospheric polar vortex are.

To answer this question, empirical orthogonal function (EOF) analysis has been carried out for 10-day-averaged Z_{50} anomalies north of 40°N obtained from the ERA-40 reanalysis (Uppala et al. 2005). Only winters (December–March) of the years 1980–2001 were considered. The average annual Z_{50} cycle has been removed beforehand. The first EOF, shown in Fig. 12, clearly reflects changes in the strength of the polar vortex. It explains 63% of the total Z_{50} variance in the domain considered. In contrast to the Z_{50} response in
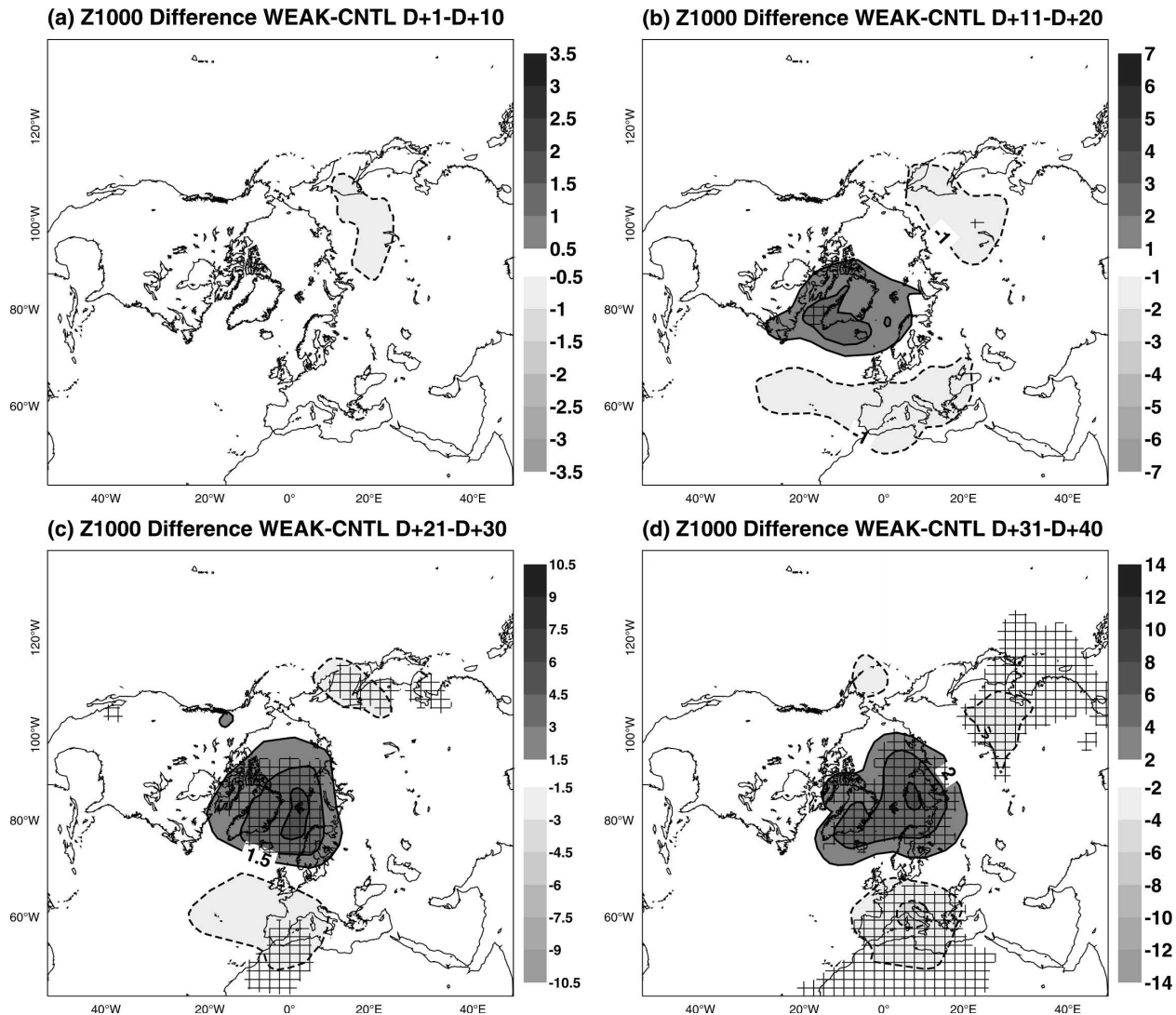
FIG. 8. As in Fig. 4 but for the 1000-hPa level.

STRONG and WEAK, however, the center, which shows anomalies of about 350 m, is located slightly closer to Greenland. The corresponding principal component (PC), by construction, is normalized to unit variance; that is, the Z_{50} anomaly shown in Fig. 12 corresponds to a value of PC = 1.0.

The smoothed cumulative probability density function (CPDF) of the first PC is shown in Fig. 13. The first thing to notice is that the PC is negatively skewed, which shows that weak polar vortex cases tend to be more extreme than strong ones (see also Monahan et al. 2003). A comparison of the response of WEAK and STRONG beyond $D + 30$ in terms of Z_{50} (Figs. 3 and 4) with the first EOF of Z_{50} anomalies (Fig. 12) reveals that the former corresponds to values of PC ± 2. From the CPDF it can be inferred that these cases are rather

extreme, although they do occur in about 1%–5% of the cases in the ERA-40 reanalysis.

4. Discussion

A recent version of the ECMWF model has been used to study the transient response of the tropospheric circulation to changes in the strength of the Northern Hemisphere stratospheric polar vortex. The focus has been on the winter season (December through March). The stratospheric polar vortex has been altered by applying a small forcing to the model's vorticity, divergence, and temperature tendencies in the stratosphere only, leaving the model formulation and the initial conditions unchanged. In agreement with previous studies (Boville 1984; Polvani and Kushner 2002; Black 2002; Ambaum and Hoskins 2002; Charlton et al. 2004) a
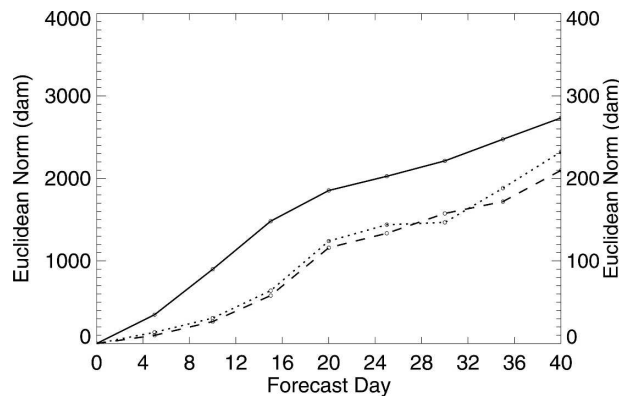
FIG. 9. Eucidean norm (dam) of the average geopotential height difference between strong (STRONG) and weak (WEAK) polar vortex cases at 50 hPa (solid), 500 hPa (dotted), and 1000 hPa (dashed) as a function of forecast time (averages from $D + 1$ to $D + 5$, $D + 6$ to $D + 10$, and so forth). Values on the left (right) ordinate refer to stratospheric (tropospheric) levels. Area weighting has been taken into account.

statistically significant response has been found throughout the troposphere, encompassing the large-scale circulation (NAO) as well as an associated change of the storm track.

It is possible that the stratosphere–troposphere connection described in this and previous studies depends on the actual state of the atmosphere. In fact, based on observational data, Perlwitz and Harnik (2004) have shown that the "downward propagation" of zonal-mean anomalies described by Baldwin and Dunkerton (2001) is stronger (weaker) for years in which the polar vortex in the lower stratosphere is anomalously weak (strong). We stratified the 60 cases available into two groups, one containing those 10 cases for which the tropospheric response to the stratospheric forcing is the strongest and the other one containing all the remaining cases. In contrast to the study of Perlwitz and Harnik (2004) we did not find any robust (statistically significant) flow
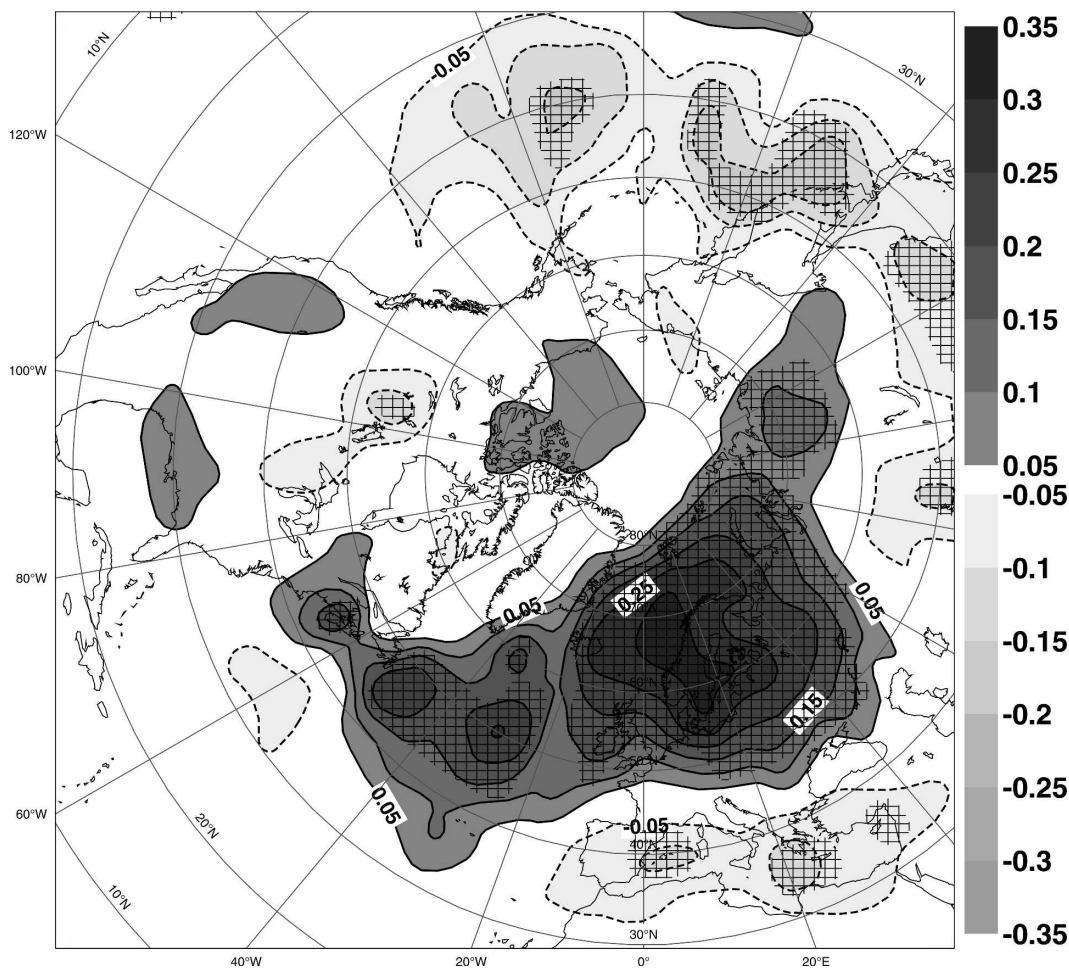

FIG. 10. Difference in synoptic activity in the range from $D + 21$ to $D + 30$ (dam day^{-1}) between STRONG and WEAK. Synoptic activity is defined as the standard deviation of day-to-day Z_{500} changes. Statistically significant differences (at the 95% confidence level) are hashed.
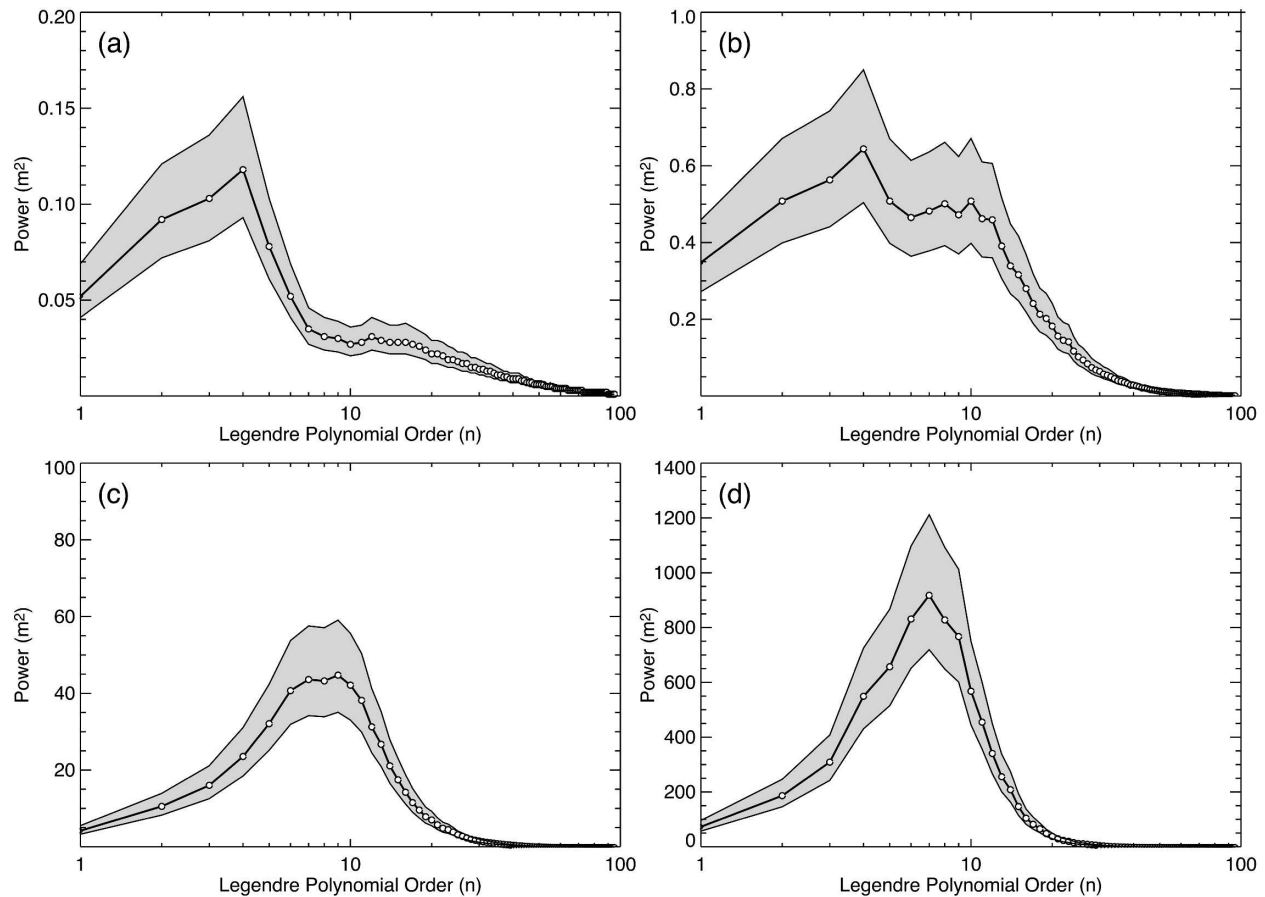
FIG. 11. Averaged power spectra (m^2; solid) of the Z_{500} difference between STRONG and WEAK as a function of total wavenumber: (a) $D + 2$, (b) $D + 4$, (c) $D + 10$, and (d) $D + 20$. For each forecast step and case (a total of 60 cases were considered), first, the power spectrum of the coefficients of the spherical harmonics has been computed. Then, the resulting 60 spectra have been averaged. Also shown are 95% confidence intervals (shaded area). Notice that the above diagnostics are global due to the use of spherical harmonics.

dependence of the stratosphere–troposhere link (not shown). It is possible that the relatively large sample size used in this study is still not large enough to detect any robust flow-dependent signal. (This would suggest that any flow dependence, if existent, is rather weak.) It is also possible, however, that the ECMWF model does not reproduce the flow dependence properly. We are planning to address this issue in future research.

The fact that a robust, transient tropospheric response to a stratospheric forcing is found in an atmospheric circulation model, which is used operationally to carry out medium-range and extended-range forecasts, is promising. However, it remains to be shown whether the stratosphere–troposphere link is strong enough to be of any practical value for extended-range predictions with numerical weather prediction models. One way to assess the skill resulting from the stratosphere–troposphere link would be to stratify hindcasts carried out with the ECMWF monthly forecasting system (Vitart 2004) into classes of strong and weak stratospheric anomalies and to assess the forecast skill for each of the two classes separately. We are planning to carry out such a study in the near future.

One novelty of the present study is the use of the adjoint technique for constructing the stratospheric forcing. One advantage of the use of the adjoint technique is that the forcing is dynamically balanced (cf. Figs. A1 and A3) and optimal; the latter allows one to keep the magnitude of the forcing relatively small. The fact that the forcing, which is optimal in changing the strength of the stratospheric polar vortex, has a large zonally symmetric component[2] is an interesting finding

---

[2] It should be pointed out that the average of all optimal adjoint forcing perturbations has been applied. The adjoint forcing perturbations for individual cases, however, resemble the mean forcing perturbation closely (not shown).
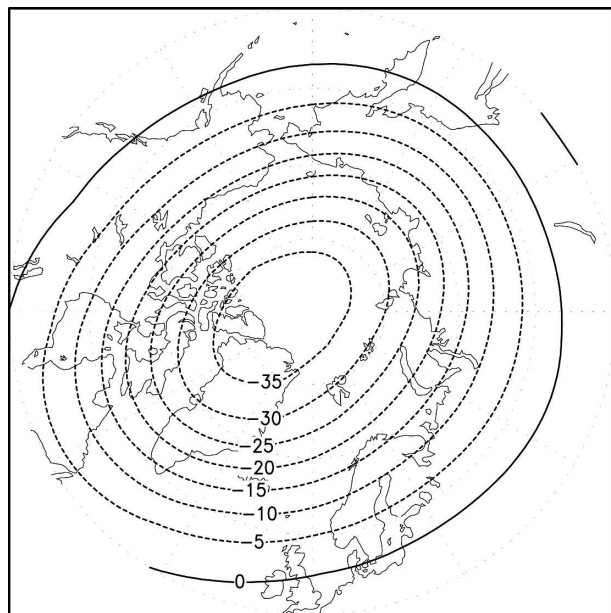
FIG. 12. First EOF of 10-day-averaged Z_{50} anomalies (dam) obtained from ERA-40 reanalysis data for all winters (Dec–Mar) of the period 1980–2001. The mean annual cycle has been removed prior to EOF analysis. Computations were carried using only data north of 40°N.
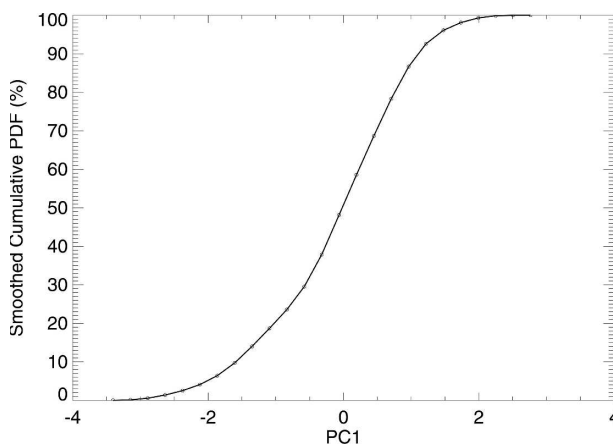

FIG. 13. Smoothed cumulative probability density function (in %) for the first PC of 10-day-averaged Z_{50} anomalies. Smoothing has been carried out using a Gaussian kernel with a window width of $h = 0.25$ (e.g., Silverman 1986).

per se, suggesting that optimal stratospheric perturbations are rather large in scale compared with those found in the troposphere (Oortwijn and Barkmeijer 1995). However, it is possible that smaller-scale structures appear if longer optimization times are used. A natural extension of the use of adjoint techniques in the context of the present study is the use of finite-time instabilities, as given by so-called singular vectors (e.g., Buizza and Palmer 1995), in studying dynamical mechanisms that may play a role in the interaction between the stratosphere and the troposphere. In recent experiments with the ECMWF model, structures were computed that transferred as much energy [see Eq. (A7)] as possible from the stratosphere to the troposphere, and vice versa (J. Barkmeijer 2006, unpublished manuscript). In contrast to the generally accepted point of view that wavenumber 1–3 should be dominant in such vertically propagating disturbances (e.g., Charney and Drazin 1961), it was found that higher wavenumbers (7–12) were far more important in transferring energy. We hope that the use of adjoint models may thus lead to new insights in the coupling between the stratosphere and troposphere and in a better understanding of, for example, stratospheric warmings.

This study also sheds some light on the nature of the stratosphere–troposphere link. First, the stratosphere–troposphere link is largely linear within a range of realistic stratospheric perturbations. Furthermore, in

agreement with previous studies (e.g., Black 2002; Ambaum and Hoskins 2002), the results presented here suggest that it is large-scale dynamics that mediate the stratosphere–troposphere link. In fact during the first few days of the integration the tropospheric response is of relatively large, supersynoptic spatial scales (wavenumber 1–6; Fig. 11a). Later throughout the forecast (e.g., at $D + 10$) most of the energy of daily Z_{500} perturbations is located on synoptic scales (Figs. 11c,d). This is not too surprising, however, given that the largest tropospheric perturbation growth during early forecast stages happens to be associated with baroclinically unstable modes (e.g., Buizza and Palmer 1995). The fact that the largest perturbations for daily fields occur on synoptic scales, therefore, does not necessarily mean that synoptic systems are crucial for *mediating* the link, as has been suggested by Charlton et al. (2004). Rather, synoptic-scale perturbations might simply be a result of the presence of large-scale anomalies—the large scale in the troposphere is modified by the stratosphere; consequently its baroclinic instability properties changes, leading to perturbation energy on synoptic scales.

APPENDIX

Construction of the Forcing

The forcing **F**, which is used to change the strength of the stratospheric polar vortex, is constructed using the

adjoint technique (e.g., Errico 1997). A brief overview of the method is given. The reader who interested in more details should consult the references given throughout this section.

Since numerical models are the basic tool of this study in order to investigate the stratosphere–troposphere link, let us start with the prognostic equation employed in numerical weather prediction,

$$d\mathbf{x}/dt = N(\mathbf{x}), \quad \text{(A1)}$$

where N is a nonlinear function. Experience from numerical weather forecasting shows that the evolution of $\mathbf{x}$ is sensitive to small perturbations, both of the initial conditions (e.g., Molteni et al. 1996) and the model tendencies (e.g., Buizza et al. 1999; Barkmeijer et al. 2003). The evolution of sufficiently small perturbations can be described by a linearized version of Eq. (A1); that is,

$$d\delta\mathbf{x}/dt \approx \mathcal{N}_L\delta\mathbf{x} + \mathbf{f}, \quad \text{(A2)}$$

where $\delta\mathbf{x}$ is a small perturbation of the atmospheric state vector (difference between perturbed and unperturbed forecast); $\mathcal{N}_L$ is the Jacobian of N; and $\mathbf{f}$ represents a small, time-dependent forcing of the model tendencies.

The solution of Eq. (A2) takes the following form (e.g., Barkmeijer et al. 2003):

$$\delta\mathbf{x}_t = \mathbf{M}(0, t)\delta\mathbf{x}_0 + \int_0^t \mathbf{M}(s, t)\mathbf{f}_s\, ds, \quad \text{(A3)}$$

where $\delta\mathbf{x}_0$ denotes a perturbation to the initial conditions; $\delta\mathbf{x}_t$ is the perturbation at final time t; and $\mathbf{M}$ is the tangent forward propagator. In this study only the case of $\delta\mathbf{x}_0 = \mathbf{0}$ (no initial perturbations) and $\mathbf{f}_s = \bar{\mathbf{f}} = \text{const}$ is considered so that Eq. (A6) reduces to

$$\delta\mathbf{x}_t = \tilde{\mathbf{M}}\bar{\mathbf{f}}, \quad \text{(A4)}$$

where $\tilde{\mathbf{M}} = \int_0^t \mathbf{M}(s, t)\, ds$. Since in nonlinear systems like Eq. (A1) the operator $\tilde{\mathbf{M}}$ depends on $\mathbf{x}$, the perturbation growths of a given optimal forcing $\bar{\mathbf{f}}$ is flow dependent (e.g., Palmer 1993).

Here, we are interested in such forcing perturbations $\bar{\mathbf{f}}$ that are efficient in changing the strength of the strato-

spheric polar vortex, that is, at final time t the evolved perturbation $\delta\mathbf{x}_t$ should project strongly onto stratospheric polar vortex anomalies ($\delta\mathbf{x}_{\text{SPV}}$, hereafter). To quantify the difference between $\delta\mathbf{x}_t$ and $\delta\mathbf{x}_{\text{SPV}}$ we use the following cost function:

$$J(\bar{\mathbf{f}}) = \frac{1}{2}\langle\mathbf{P}(\tilde{\mathbf{M}}\bar{\mathbf{f}} - \delta\mathbf{x}_{\text{SPV}}), \mathbf{C}_F\mathbf{P}(\tilde{\mathbf{M}}\bar{\mathbf{f}} - \delta\mathbf{x}_{\text{SPV}})\rangle. \quad \text{(A5)}$$

Here $\mathbf{P}$ denotes the projection operator (Buizza 1994), which is used for localization in space; angle brackets represent the Euclidean inner product; and $\mathbf{C}_F$ induces a norm at final time t. The ultimate aim is to find that $\bar{\mathbf{f}}$, which minimizes the cost function J.

To solve the minimization problem we use a second-order quasi-Newton method (Gilbert and Lemarechal 1989). This requires knowledge of the gradient of J with respect to the forcing perturbation $\bar{\mathbf{f}}$, which can be obtained as follows (e.g., Oortwijn and Barkmeijer 1995; Rabier et al. 1996; Barkmeijer et al. 2003 for details):

$$\nabla_{\bar{\mathbf{f}}}J = \mathbf{C}_E^{-1}\tilde{\mathbf{M}}^T\mathbf{P}^T\mathbf{C}_F\mathbf{P}(\tilde{\mathbf{M}}\bar{\mathbf{f}} - \delta\mathbf{x}_{\text{SPV}}). \quad \text{(A6)}$$

This gradient—also sometimes referred to as the *sensitivity* (Oortwijn and Barkmeijer 1995; Rabier et al. 1996)—depends on (i) the pattern being investigated (here, $\delta\mathbf{x}_{\text{SPV}}$), the tangent linear propagator $\tilde{\mathbf{M}}$ and its adjoint $\tilde{\mathbf{M}}^T$, and, therefore, (ii) the actual flow, (iii) the area being targeted, and (iv) the norms being used at initial and final time ($\mathbf{C}_E$ and $\mathbf{C}_F$, respectively).

In this study, an optimization time of $t = 48$ h is used. The focus is on the Northern Hemisphere and localization is achieved by using the projection operator, which sets all values south of 30°N effectively to zero. Diabatic versions of $\tilde{\mathbf{M}}$ and $\tilde{\mathbf{M}}^T$ are used at a horizontal resolution of T63 and with 60 levels in the vertical. The linearized physics are the same as in Mahfouf (1999) comprising vertical diffusion, large-scale condensation, longwave radiation, deep cumulus convection, and subgrid-scale orographic effects. The minimization of the cost function is based on six iterations (see Klinker et al. 1998 for further details).

The total energy norm is used for $\mathbf{C}_E$ and $\mathbf{C}_F$, which is defined as follows:

$$\langle\mathbf{x}, C_{\text{TE}}\mathbf{x}\rangle = \frac{1}{2}\int\int\left[u'^2 + v'^2 + \frac{c_p}{T_r}T'^2 + c_q\frac{L^2}{c_pT_r}q'^2\right]d\Sigma\frac{\partial p_r}{\partial\eta}d\eta + \frac{1}{2}\int\left[R\frac{T_r}{p_r}\ln p_s'^2\right]d\Sigma, \quad \text{(A7)}$$

where u', v', T', p_s', and q' are perturbations of zonal wind, meridional wind, temperature, surface pressure, and humidity, respectively (e.g., Ehrendorfer et al. 1999 for details). The integration is carried out over the

whole horizontal domain $\hat{\Sigma}$ and all vertical levels η. In this study $c_q = 0.0$ so that Eq. (A7) reduces to the *dry* total energy norm.
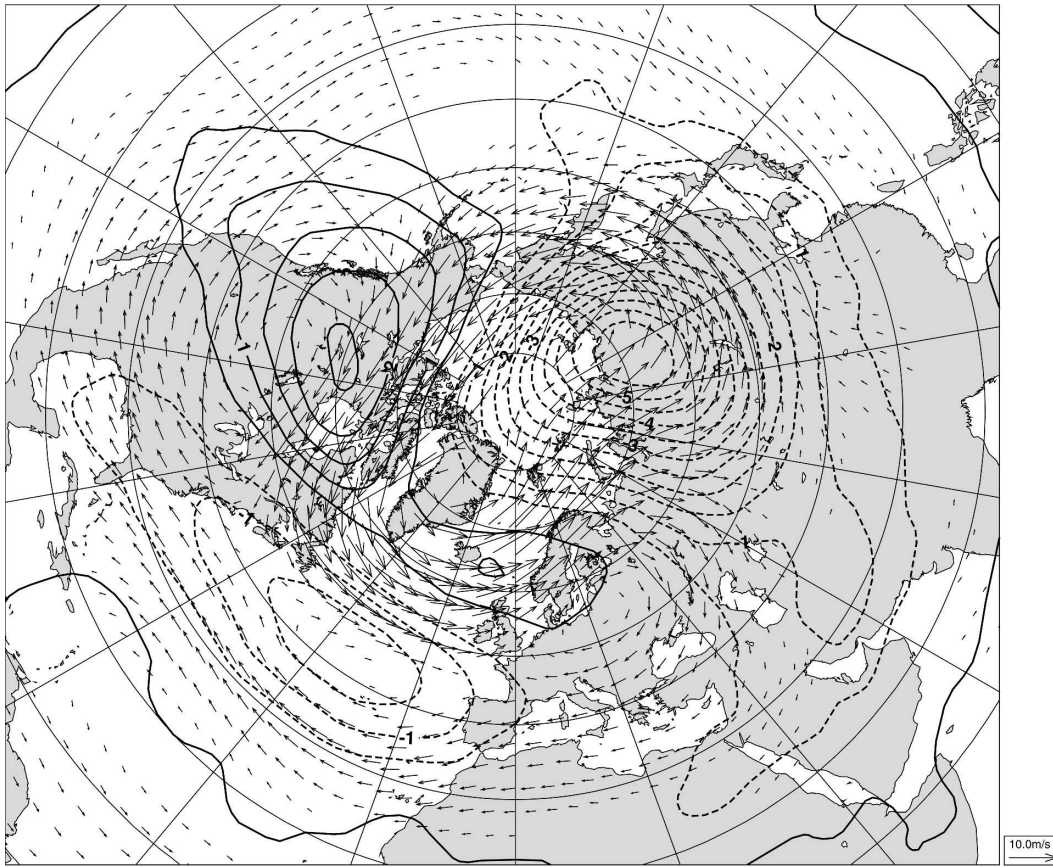
The pattern used to representing stratospheric polar

FIG. A1. Anomalous wind (m s^{-1}) and temperature (contour interval is 0.5 K) fields at about 50 hPa associated with the positive phase of the NAO during wintertime (Dec–Mar). Positive (negative) temperature contours are solid (dashed). Results are based on compositing monthly mean ERA-40 data at model level 22 (about 50 hPa) according to the monthly mean value of the observed NAO index.

vortex anomalies is based on the full three-dimensional state vector of the NAO, that is, $\delta\mathbf{x}_{\mathrm{SPV}} \equiv \delta\mathbf{x}_{\mathrm{NAO}}$. Recall that the state vector encompasses vorticity, divergence, temperature, the logarithm of surface pressure, and specific humidity on all 60 model levels. To construct this pattern we have made use of ERA-40 reanalysis data (Uppala et al. 2005) truncated at T63 in order to match the resolution used for minimization. First, the NAO index has been constructed for each of the months from December to March of the period 1958–2001 by taking the difference between normalized monthly mean sea level pressure time series from the Azores and Iceland (Walker 1924; Hurrell 1995a). Then high and low NAO composites have been formed by averaging all monthly mean state vectors for which the NAO index is one standard deviation above and below normal, respectively. The NAO pattern, $\delta\mathbf{x}_{\mathrm{NAO}}$, used during the course of the minimization is the difference between the high and low NAO composites. Both the NAO index and the three-dimensional state vector are

based on ERA-40 reanalysis data (truncated at T63). The NAO pattern is shown Fig. A1 for anomalous horizontal wind vectors and temperatures at about 50 hPa. Evidently, it reflects an anomalously strong and cold polar vortex.
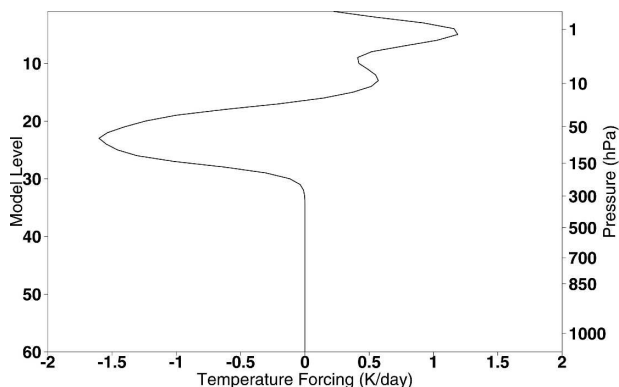

FIG. A2. Vertical profile of the mean temperature forcing (K day^{-1}) averaged over the area 60°–90°N, 50°–140°E.
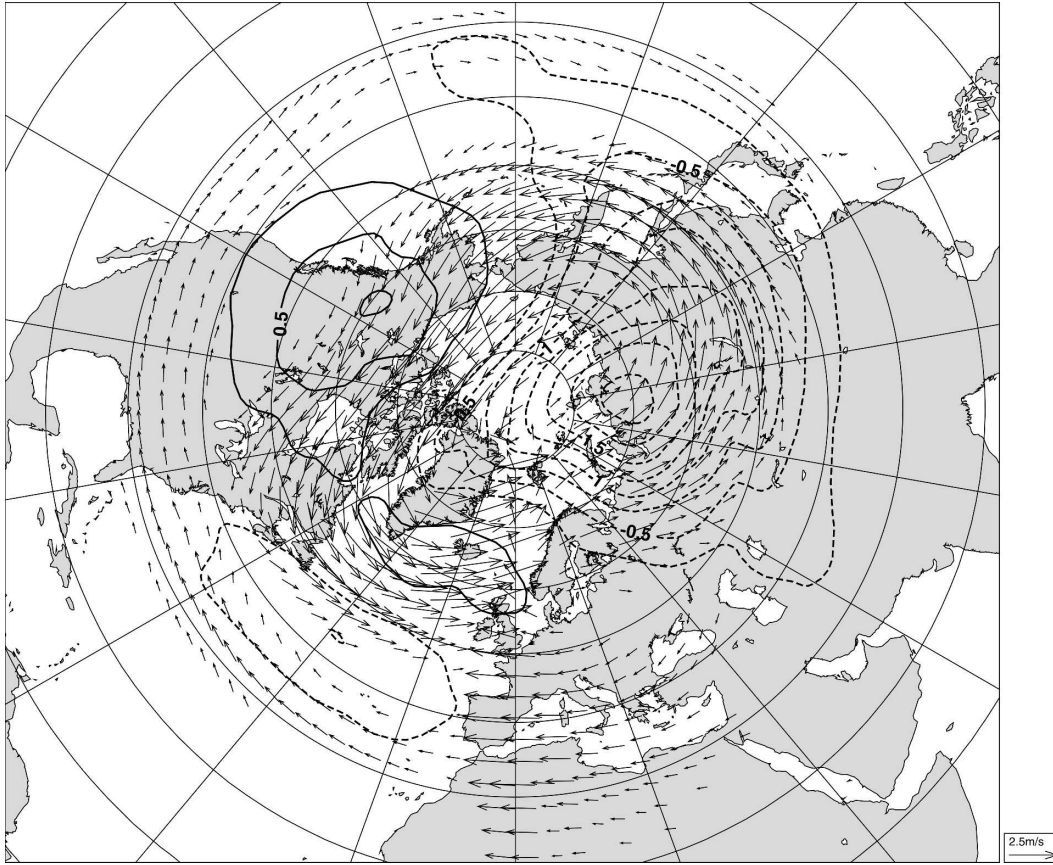
FIG. A3. Mean wind (m s^{-1} day^{-1}) and temperature (contour interval is 0.25 K day^{-1}) forcing at about 50 hPa based on 19 adjoint forcing patterns. This stratospheric forcing is used throughout this study to change the strength of the stratospheric polar vortex. A reference arrow for the wind forcing is also given. Wind forcing vectors with a magnitude below 0.5 m s^{-1} day^{-1} have been omitted. Positive (negative) temperature forcing contours are solid (dashed).

Next, this pattern has been used to construct optimal forcing perturbations, $\bar{\mathbf{f}}$, for 19 days (each 5 days apart) in the winter 2002/03 using the method outlined above. Then, all of the 19 optimal forcing patterns have been averaged to obtain the forcing for the nonlinear model, that is, $\mathbf{F} = \langle\bar{\mathbf{f}}\rangle$, where now the angle brackets denote ensemble averaging. The forcing $\mathbf{F}$ has been set to zero below model level 27 (about 150 hPa) in order to restrict the forcing to the stratosphere only. The transition from nonzero to zero forcing has been slightly smoothed to prevent the generation of a spurious potential vorticity forcing in the lower stratosphere. The vertical profile of the resulting temperature forcing averaged over the area 60°–90°N, 50°–140°E is shown in Fig. A2. The largest temperature forcing, which leads to an *increase* of the stratospheric polar vortex, appears in the lower stratosphere between about 150 to 50 hPa amounting to −1.0 to −1.5 K day^{-1}. Moreover, Fig. A2 highlights the fact that the troposphere remains unperturbed.

The wind and temperature forcing at about 50 hPa, which should be efficient in *increasing* the strength of the stratospheric polar vortex is shown in Fig. A3. The first thing to notice is that this pattern is very similar to the NAO pattern used as input to the adjoint (see Fig. A1). There is, however, a shift of about 20° to the west in the temperature forcing field compared to the temperature anomaly associated with the NAO. The forcing basically slightly shifts, accelerates, and cools the stratospheric polar vortex. Moreover, it is evident that the forcing magnitude is relatively small amounting to about 2.5 m s^{-1} day^{-1} for wind speed and 2 K day^{-1} for temperature.

REFERENCES

Ambaum, M. H. P., and B. J. Hoskins, 2002: The NAO troposphere–stratosphere connection. *J. Climate,* **15,** 1969–1978.

Baldwin, M. P., and T. J. Dunkerton, 1999: Propagation of the Arctic Oscillation from the stratosphere to the troposphere. *J. Geophys. Res.,* **104,** 30 937–30 946.

——, and ——, 2001: Stratospheric harbingers of anomalous weather regimes. *Science,* **294,** 581–584.

——, D. B. Stephenson, D. W. J. Thompson, T. J. Dunkerton, A. J. Charlton, and A. O'Neill, 2003: Stratospheric memory and skill of extended-range weather forecasts. *Science,* **301,** 636–640.

Barkmeijer, J., T. Iversen, and T. N. Palmer, 2003: Forcing singular vectors and other sensitive model structures. *Quart. J. Roy. Meteor. Soc.,* **129,** 2401–2423.

Black, R. X., 2002: Stratospheric forcing of surface climate in the Arctic Oscillation. *J. Climate,* **15,** 268–277.

Boville, B. A., 1984: The influence of the polar night jet in the tropospheric circulation in a GCM. *J. Atmos. Sci.,* **41,** 1132–1142.

Buizza, R., 1994: Localization of optimal perturbations using a projection operator. *Quart. J. Roy. Meteor. Soc.,* **120,** 1647–1682.

——, and T. Palmer, 1995: The singular-vector structure of the atmospheric global circulation. *J. Atmos. Sci.,* **52,** 1434–1456.

——, M. Miller, and T. N. Palmer, 1999: Stochastic representation of model uncertainties in the ECWMF Ensemble Prediction System. *Quart. J. Roy. Meteor. Soc.,* **125,** 2887–2908.

Charlton, A. J., A. O. O'Neill, D. B. Stephenson, W. A. Lahoz, and M. P. Baldwin, 2003: Can knowledge of the state of the stratosphere be used to improve statistical forecasts of the troposphere? *Quart. J. Roy. Meteor. Soc.,* **129,** 3205–3225.

——, ——, W. A. Lahoz, and A. C. Massacand, 2004: Sensitivity of tropospheric forecasts to stratospheric initial conditions. *Quart. J. Roy. Meteor. Soc.,* **130,** 1771–1792.

Charney, J. G., and P. G. Drazin, 1961: Propagation of planetary-scale disturbances from the lower into the upper atmosphere. *J. Geophys. Res.,* **66,** 83–109.

Ehrendorfer, M., R. Errico, and K. Raeder, 1999: Singular-vector perturbation growth in a primitive equation model with moist physics. *J. Atmos. Sci.,* **56,** 1627–1648.

Errico, R. M., 1997: What is an adjoint model? *Bull. Amer. Meteor. Soc.,* **78,** 2577–2591.

Gilbert, J. C., and C. Lemarechal, 1989: Some numerical experiments with variable-storage quasi-Newton algorithms. *Math. Program.,* **45,** 407–435.

Hurrell, J. W., 1995a: Decadal trends in the North Atlantic Oscillation: Regional temperatures and precipitation. *Science,* **269,** 676–679.

——, 1995b: Transient eddy forcing of the rotational flow during northern winter. *J. Atmos. Sci.,* **52,** 2286–2301.

Jung, T., 2005: Systematic errors of the atmospheric circulation in the ECMWF forecasting system. *Quart. J. Roy. Meteor. Soc.,* **131,** 1045–1073.

——, and A. M. Tompkins, 2003: Systematic errors in the ECMWF forecasting system. Tech. Rep. 422, ECMWF, Shinfield Park, Reading, United Kingdom, 74 pp.

Klinker, E., F. Rabier, and R. Gelaro, 1998: Estimation of key analysis errors using the adjoint technique. *Quart. J. Roy. Meteor. Soc.,* **124,** 1909–1933.

Kodera, K., M. Chiba, K. Yamazaki, and K. Shibata, 1991: A possible influence of the polar night stratospheric jet on the subtropical tropospheric jet. *J. Meteor. Soc. Japan,* **69,** 715–720.

Mahfouf, J.-F., 1999: Influence of physical processes on the tangent-linear approximation. *Tellus,* **51A,** 147–166.

Molteni, F., R. Buizza, T. N. Palmer, and T. Petroliagis, 1996: The ECMWF ensemble prediction system: Methodology and validation. *Quart. J. Roy. Meteor. Soc.,* **122,** 73–119.

Monahan, A. H., J. C. Fyfe, and L. Pandolfo, 2003: The vertical structure of wintertime climate regimes of the Northern Hemisphere extratropical atmosphere. *J. Climate,* **16,** 2005–2021.

Norton, W. A., 2003: Sensitivity of Northern Hemisphere surface climate to simulation of the stratospheric polar vortex. *Geophys. Res. Lett.,* **30,** 1627, doi:10.1029/2003GL016958.

Oortwijn, J., and J. Barkmeijer, 1995: Perturbations that optimally trigger weather regimes. *J. Atmos. Sci.,* **52,** 3932–3944.

Palmer, T. N., 1993: Extended-range atmospheric prediction and the Lorenz model. *Bull. Amer. Meteor. Soc.,* **74,** 49–65.

Perlwitz, J., and N. Harnik, 2004: Downward coupling between the stratosphere and troposphere: The relative roles of wave and zonal mean processes. *J. Climate,* **17,** 4902–4909.

Polvani, L. M., and P. J. Kushner, 2002: Tropospheric response to stratospheric perturbations in a relatively simple general circulation model. *Geophys. Res. Lett.,* **29,** 1114, doi:10.1029/2001GL014284.

Rabier, F., E. Klinker, P. Courtier, and A. Hollingsworth, 1996: Sensitivity of forecast errors to initial conditions. *Quart. J. Roy. Meteor. Soc.,* **122,** 121–150.

Silverman, B. W., 1986: *Density Estimation for Statistics and Data Analysis.* Chapman and Hall/CRC, 175 pp.

Taguchi, M., 2003: Tropospheric response to stratospheric degradation in a simple global circulation model. *J. Atmos. Sci.,* **60,** 1835–1846.

Thompson, D. W. J., and J. M. Wallace, 1998: The Arctic Oscillation signature in the wintertime geopotential height and temperature fields. *Geophys. Res. Lett.,* **25,** 1297–1300.

Ting, M., and N.-C. Lau, 1993: A diagnostic and modeling study of the monthly mean wintertime anomalies appearing in a 100-year GCM experiment. *J. Atmos. Sci.,* **50,** 2845–2867.

Untch, A., and A. J. Simmons, 1999: Increased stratospheric resolution. *ECMWF Newsletter,* No. 82, ECMWF, Reading, United Kingdom, 3–8.

Uppala, S., and Coauthors, 2005: The ERA-40 reanalysis. *Quart. J. Roy. Meteor. Soc.,* **131,** 2561–3012.

Vitart, F., 2004: Monthly forecasting at ECMWF. *Mon. Wea. Rev.,* **132,** 2761–2779.

Walker, G. T., 1924: Correlation in seasonal variation of weather, IX. *Mem. Indian. Meteor. Dep.,* **24** (9), 275–332.

Wittman, M. A. H., L. M. Polvani, R. K. Scott, and A. J. Charlton, 2004: Stratospheric influence on baroclinic lifecycles and its connection to the Artic Oscillation. *Geophys. Res. Lett.,* **31,** L16113, doi:10.1029/2004GL020503.